Combined Bluntness and Roughness Effects on Cones at Hypersonic Speeds

P. Paredes,[1] A. Scholten,[2] M. Choudhari,[3] F. Li,[3]
B. Prince,[4] J. Jewell[4]

[1]National Institute of Aerospace

[2]North Carolina State University

[3]Computational AeroSciences Branch, NASA Langley Research Center

[4]Purdue University

AIAA Aviation 2022, 27 June-1 July, 2022, Chicago, IL

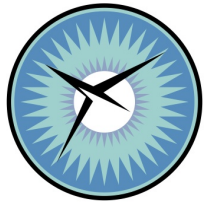

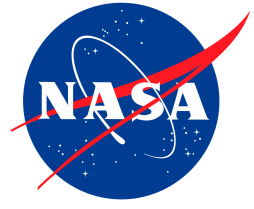

Outline

Outline

Flow over Blunt Cones at Supersonic/Hypersonic Speeds

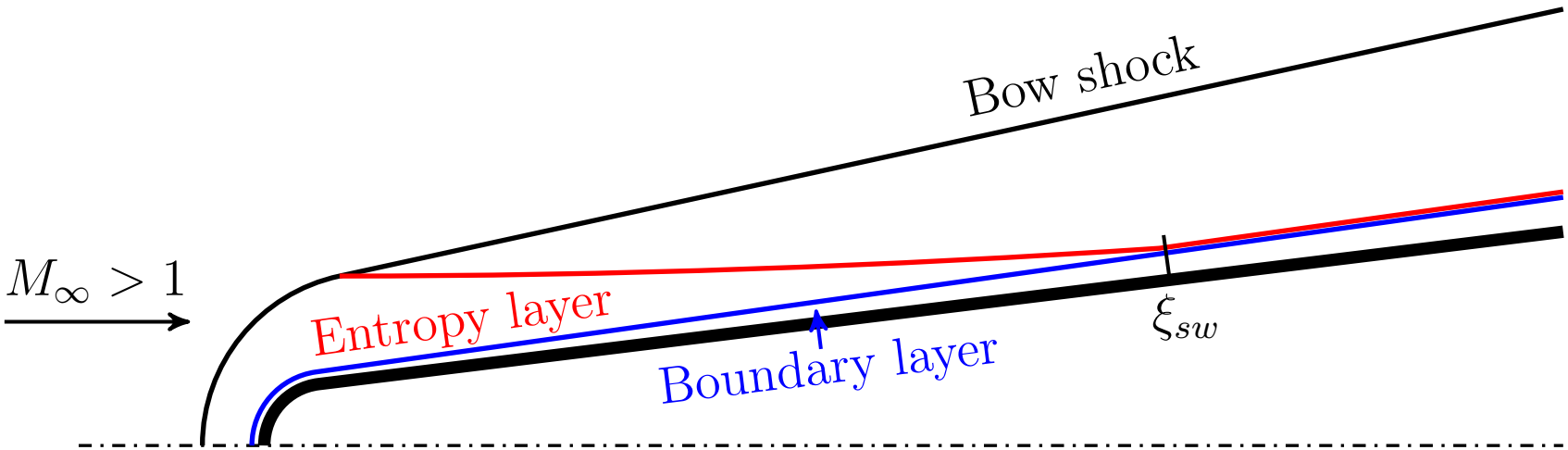

Transition Measurements over Blunt Cones[1]

- Transition Reynolds number (Re_{ξ_T}) vs. nose Reynolds number (Re_{R_N})
  - Mach 6. (A) Stetson (1983), (B) Aleksandrova et al. (2014).
  - Mach 9 to 10. (C) Stetson (1983), (D) Marineau et al. (2014), (E) Softley et al. (1969).

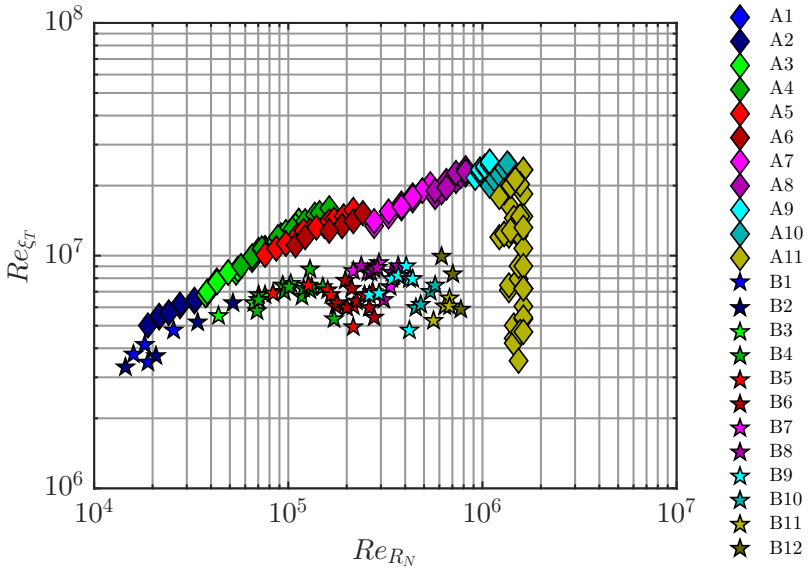

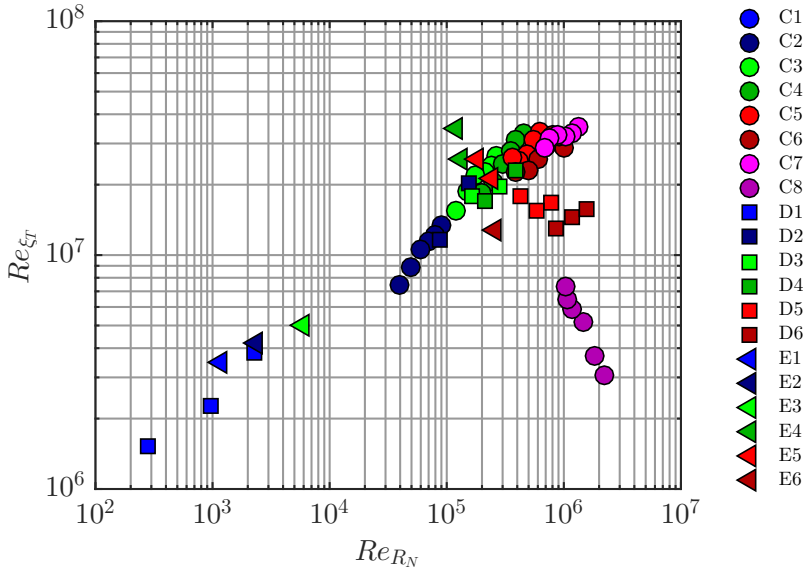

- Small bluntness: transition location moves downstream with increasing R_N
- Large bluntness: transition location rapidly moves upstream (Transition Reversal)
- Differences in critical Re_{R_N} attributed to uncontrolled nosetip roughness

[1] P. Paredes et al. "Nosetip bluntness effects on transition at hypersonic speeds: experimental and numerical analysis". In: *Journal of Spacecraft Rockets* 56.2 (2019). DOI: 10.2514/1.A34277.

Effect of nose bluntness at fixed $Re_{kk} \approx 300$

- AFRL Mach 6 High Reynolds number facility[2]
- 7° half-angle cone at zero AoA; $R_N = 5.080$ mm, $R_N = 15.24$ mm
- Array of 15 μm cubical, laser-machined roughness elements at $\theta = 45^\circ$ ($M_e \approx 1$)
- Number of elements (m) set to maximum transient growth within nosetip:
  - $R_N = 5.08$ mm, $Re_\infty \approx 66 \times 10^6$ m^{-1}: $m = 210$, $k/\delta_h = 0.381$
  - $R_N = 15.24$ mm, $Re_\infty \approx 76 \times 10^6$ m^{-1}: $m = 420$, $k/\delta_h = 0.225$

- Mach number contours and sonic line

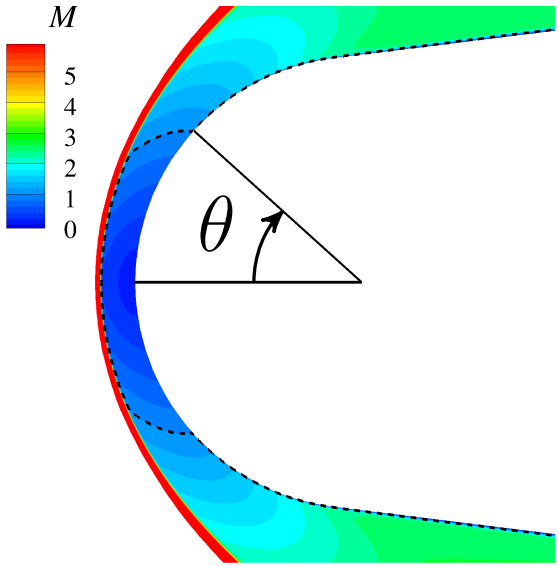

- Picture of rough nosetip

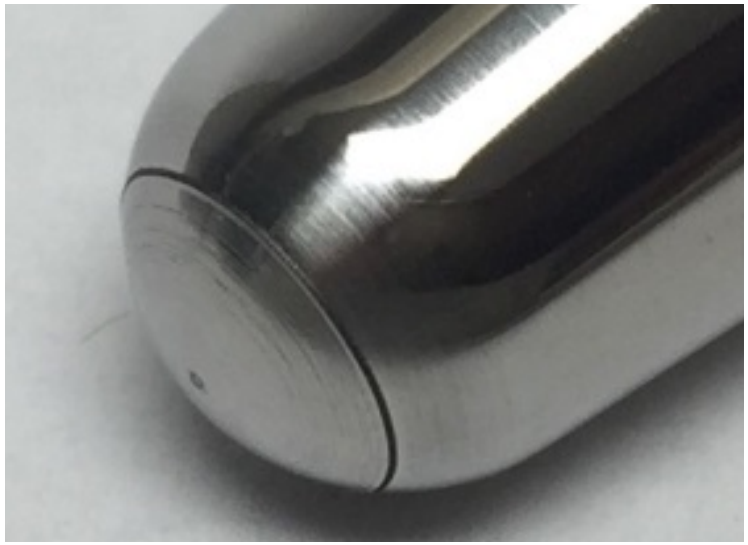

[2] P. Paredes et al. "Nosetip bluntness effects on transition at hypersonic speeds: experimental and numerical analysis". In: *Journal of Spacecraft Rockets* 56.2 (2019). DOI: 10.2514/1.A34277.

Effect of nose bluntness at fixed $Re_{kk} \approx 300$

- AFRL Mach 6 High Reynolds number facility
- 7° half-angle cone at zero AoA; $R_N = 5.080$, 15.24 mm
- Array of 15 μm cubical, laser-machined roughness elements at $\theta = 45^\circ$
  - $R_N = 5.08$ mm, $m = 210$, $k/\delta_h = 0.381$
  - $R_N = 15.24$ mm, $m = 420$, $k/\delta_h = 0.225$

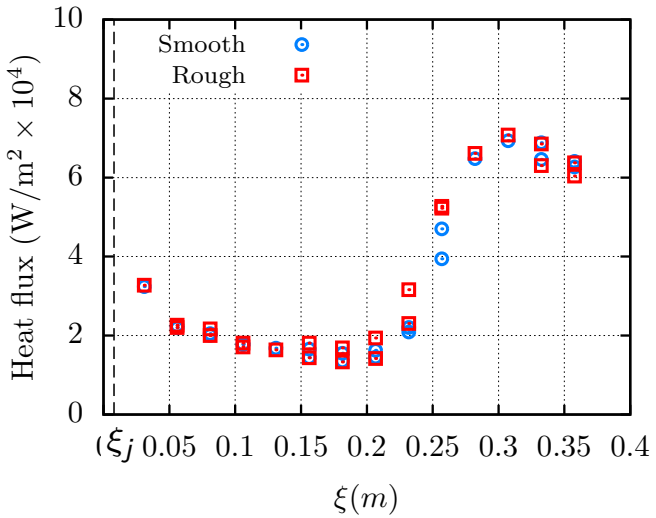

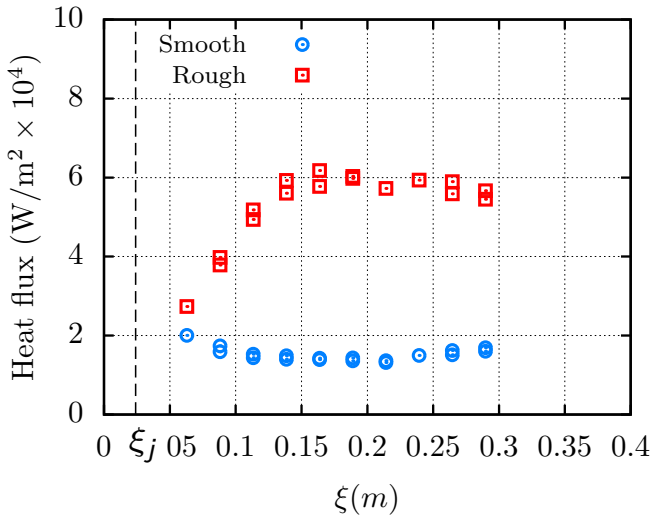

- **Small bluntness**: Roughness has no effect on ξ_T
- **Large bluntness**: Rough tip moves ξ_T from the end of the cone to $\approx \xi_j$
- **Transition onset associated with combined effects of bluntness and roughness**

Outline

Computational Analysis

Stability Theory

Linear Stability Analysis

- Decomposition of flow variables:

$$\mathbf{q}(\xi,\eta,\zeta,t) = \bar{\mathbf{q}}(\xi,\eta,\zeta) + \epsilon\tilde{\mathbf{q}}(\xi,\eta,\zeta,t); \quad \bar{\mathbf{q}} = \mathcal{O}(1); \quad \epsilon \ll 1$$

- Harmonic LNSE (HLNSE): 3D linear system of equations
  - Exploit basic state independence w.r.t. time

$$\tilde{\mathbf{q}}(\xi,\eta,\zeta,t) = \breve{\mathbf{q}}(\xi,\eta,\zeta)\exp\left[-\mathrm{i}\left(\omega t\right)\right]$$

$$\mathbf{L}_{HLNSE}\hat{\mathbf{q}}(\xi,\eta,\zeta) = \breve{\mathbf{f}}(\xi,\eta,\zeta)$$

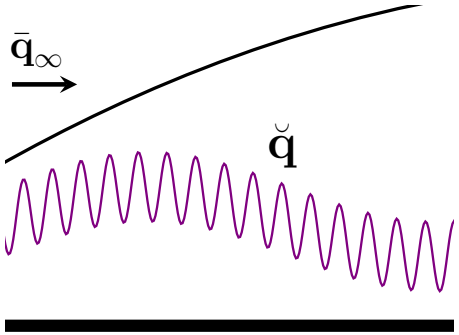

- Plane-marching PSE: Parabolic integration in ξ with 2D linear systems
  - Exploit slow variations in streamwise direction in roughness wake

$$\breve{\mathbf{q}}(\xi,\eta,\zeta) = \hat{\mathbf{q}}(\xi,\eta,\zeta)\theta(\xi);\ \theta(\xi) = \exp\left[\mathrm{i}\int_{\xi_0}^{\xi}\alpha(\xi')\,\mathrm{d}\xi'\right]$$

$$\mathbf{L}_{PSE}(\alpha)\hat{\mathbf{q}}(\xi,\eta,\zeta) = 0 \ \&\ \int_{\eta,\zeta}\hat{\mathbf{q}}^*\frac{\partial\hat{\mathbf{q}}}{\partial\xi}\,h_\xi\,h_\zeta\,\mathrm{d}\zeta\,\mathrm{d}\eta = 0$$

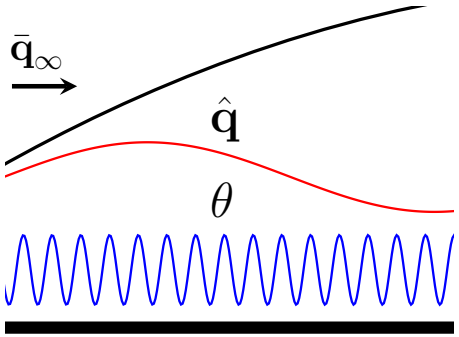

Inflow-Resolvent Analysis based on 3D HLNSE

- Inflow-resolvent analysis commonly used for 2D/axisymmetric configurations[3,4]
- Optimal inflow disturbance, $\tilde{\mathbf{q}}_0 = \tilde{\mathbf{q}}(\xi_0)$ that maximizes J:
  - Outlet energy gain: $J = G_E^{out} = \frac{E(\xi_1)}{E(\xi_0)}$
- Energy norm: $E(\xi) = \int_\eta \tilde{\mathbf{q}}(\xi)^* \mathbf{M}(\xi) \tilde{\mathbf{q}}(\xi)\, h_\xi\, h_\zeta\, \mathrm{d}\eta$

$$\mathbf{M}(\xi) = \mathrm{diag}\left[\frac{\bar{T}(\xi)}{\gamma \bar{\rho}(\xi) M^2}, \bar{\rho}(\xi), \bar{\rho}(\xi), \bar{\rho}(\xi), \frac{\bar{\rho}(\xi)}{\gamma(\gamma-1)\bar{T}(\xi) M^2}\right]$$

- Variational formulation using direct and adjoint eqs: $\mathcal{L}(\tilde{\mathbf{q}}, \tilde{\mathbf{q}}^\dagger) = J(\tilde{\mathbf{q}}) - \langle \tilde{\mathbf{q}}^\dagger, \mathbf{L}\tilde{\mathbf{q}} \rangle$
- Application to incompressible axisymmetric jet

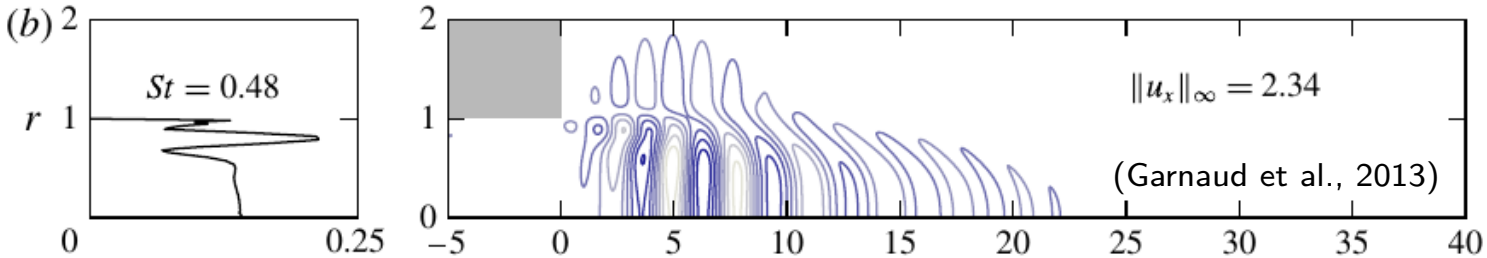

[3] X. Garnaud et al. "The preferred mode of incompressible jets: Linear frequency response analysis". In: *Journal of Fluid Mechanics* 716 (2013), pp. 189–202. DOI: 10.1017/jfm.2012.540.

[4] P. Paredes et al. "Nosetip bluntness effects on transition at hypersonic speeds: experimental and numerical analysis". In: *Journal of Spacecraft Rockets* 56.2 (2019). DOI: 10.2514/1.A34277.

Computational Analysis

Results

Boundary-Layer Flow

- Unperturbed, axisymmetric flow
  - Computed with the NASA VULCAN-CFD solver[5]
  - 7° half-angle cone with $R_N = 15.24$ mm at zero AoA
  - $M_\infty = 5.9$, $Re_\infty = 75.8 \times 10^6$ m^{-1}, $T_\infty = 76.74$ K, $T_w/T_{w,ad} = 0.57$
- Perturbed, 3D flow
  - Computed with high-order DNS solver[6]
  - Roughness elements designed based on experiments[7]
    - $\theta = 45°$ ($M_e = 1.1$), $m = 420$, $k = 15$ μm and 20 μm
    - Cubic and prismatic elements (50% blockage)
- Roughness parameters for both k are supercritical based on both the ballistics-range data (Reda, 2002) and a transient growth correlation (Reshotko & Tumin, 2004)

k [μm]	k/δ_h	k/Θ	Re_k **250**	Re_{kk} **250**	$Re_\Theta(k/\Theta\, T_e/T_w)^{1.3}$ **574**	$Re_\Theta(k/\Theta)(T_e/T_w)^{1.27}$ **434**
15	0.208	2.01	415	337	834	667
20	0.277	2.68	616	482	1,213	889

[5] R. Baurle et al. *VULCAN-CFD Theory Manual: Ver. 7.1.0*. NASA TM-2020-5000766. 2020.

[6] M. Wu and M.P. Martin. "Direct numerical simulation of supersonic boundary layer over a compression ramp". In: *AIAA Journal* 45.4 (2007), pp. 879–889. DOI: 10.2514/1.27021.

[7] P. Paredes et al. "Nosetip bluntness effects on transition at hypersonic speeds: experimental and numerical analysis". In: *Journal of Spacecraft Rockets* 56.2 (2019). DOI: 10.2514/1.A34277.

Boundary-Layer Flows with Roughness Elements

- Roughness elements at $\theta = 45^\circ$ with $m = 420$ on $R_N = 15.24$ mm cone
- Three-dimensional view of 3 azimuthal wavelengths with Mach number contours at selected streamwise locations
  - $k = 15$ μm, Cubic
  - $k = 15$ μm, Prismatic

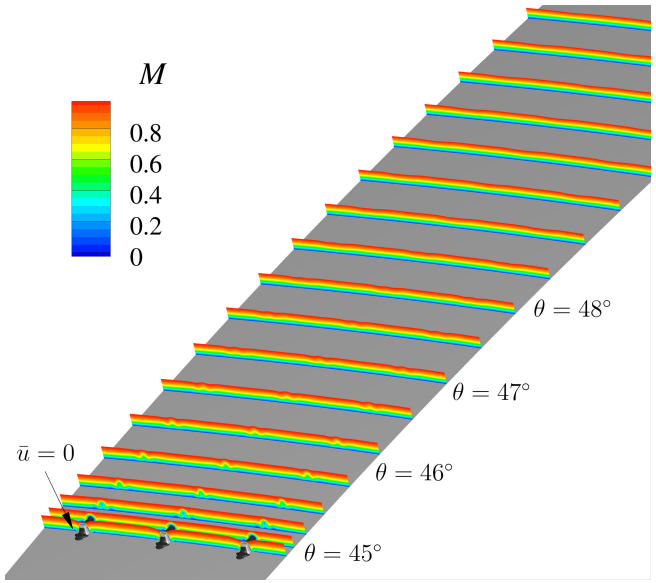

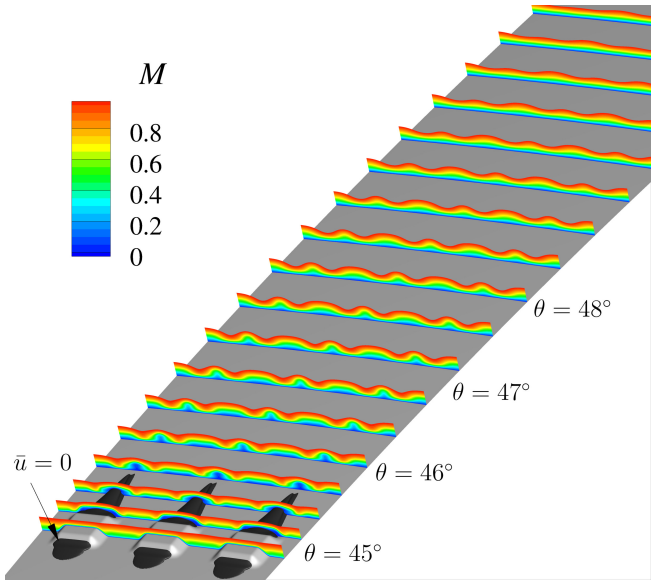

- Cubic: azimuthal variations do not spread and have short extent[8]
- Prismatic: azimuthal variations spread through the azimuthal wavelength and have a much longer streamwise extend

[8] A. Theiss et al. *Wake flow instability studies behind discrete roughness elements on a generic re-entry capsule*. AIAA Paper 2016-4382. 2016.

Boundary-Layer Flows with Roughness Elements

- Roughness elements at $\theta = 45^\circ$ with $m = 420$ on $R_N = 15.24$ mm cone
- Three-dimensional view of 3 azimuthal wavelengths with Mach number contours at selected streamwise locations
  - $k = 20$ μm, Cubic
  - $= 20$ μm, Prismatic

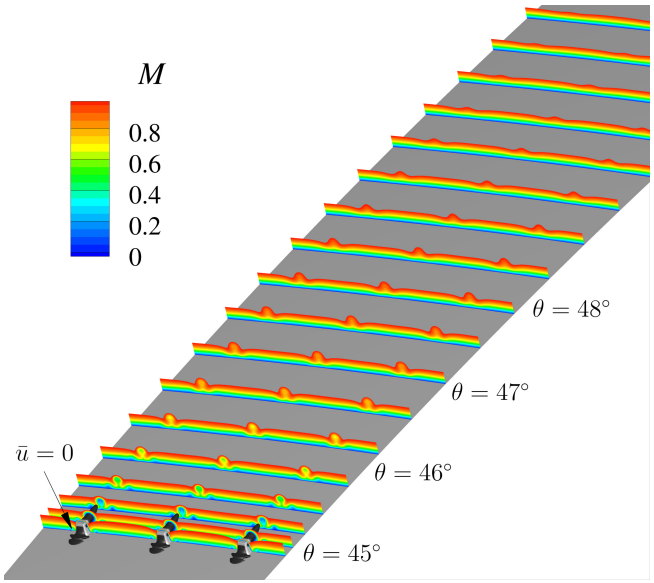

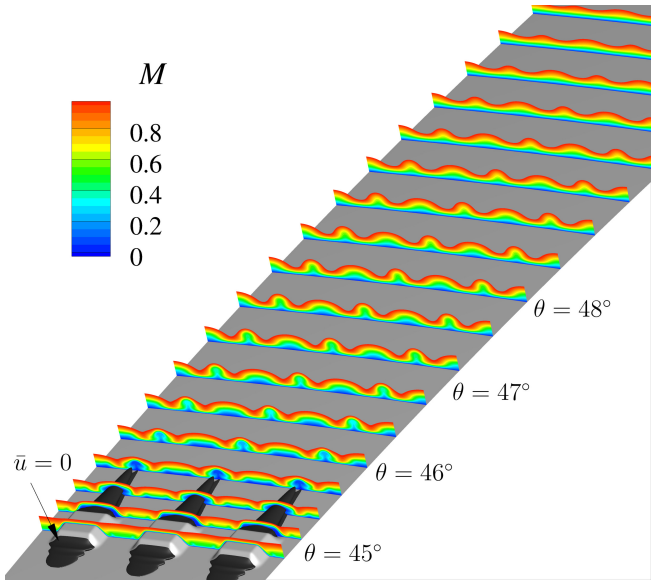

- Cubic: azimuthal variations do not spread and have short extent[8]
- Prismatic: azimuthal variations spread through the azimuthal wavelength and have a much longer streamwise extend

[8] A. Theiss et al. *Wake flow instability studies behind discrete roughness elements on a generic re-entry capsule*. AIAA Paper 2016-4382. 2016.

Plane-Marching PSE Analysis of Roughness Wakes

- Roughness elements at $\theta = 45^\circ$ with $m = 420$ on $R_N = 15.24$ mm cone
- Stable and robust integration of PSE only downstream of separation region
- N-factor curves for symmetric (SS, AS) and antisymmetric (AA, SA) modes
  - $k = 15$ μm, Cubic

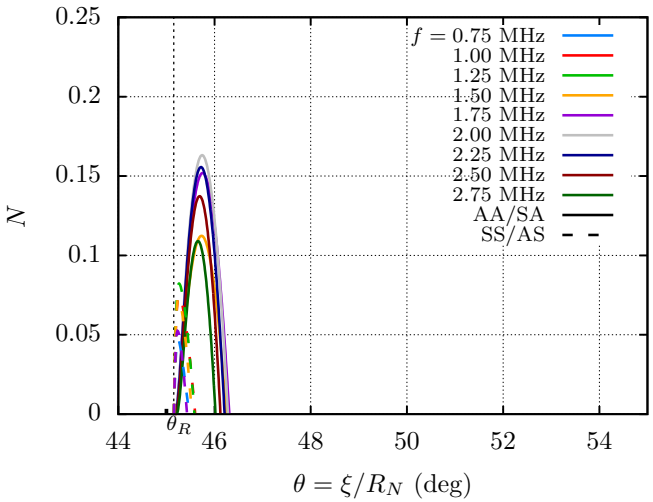

  - $k = 15$ μm, Prismatic

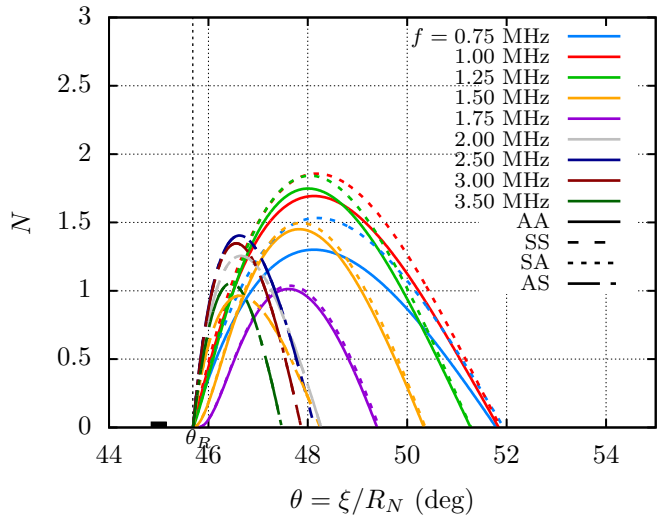

- Disturbance amplification occurs within few degrees from the roughness element
- Highest growth rates at reattachment location (θ_R) for most amplified modes
- Cubic, 15 μm: Marginally amplified with $N_{max} \approx 0.16$ for AA/SA with $f = 2.0$ MHz
- Prismatic, 15 μm: Larger $N_{max} \approx 1.9$ for SA with $f = 1.0$ MHz

Plane-Marching PSE Analysis of Roughness Wakes

- Roughness elements at $\theta = 45^\circ$ with $m = 420$ on $R_N = 15.24$ mm cone
- Stable and robust integration of PSE only downstream of separation region
- N-factor curves for symmetric (SS, AS) and antisymmetric (AA, SA) modes
  - $k = 20$ μm, Cubic
  - $k = 20$ μm, Prismatic

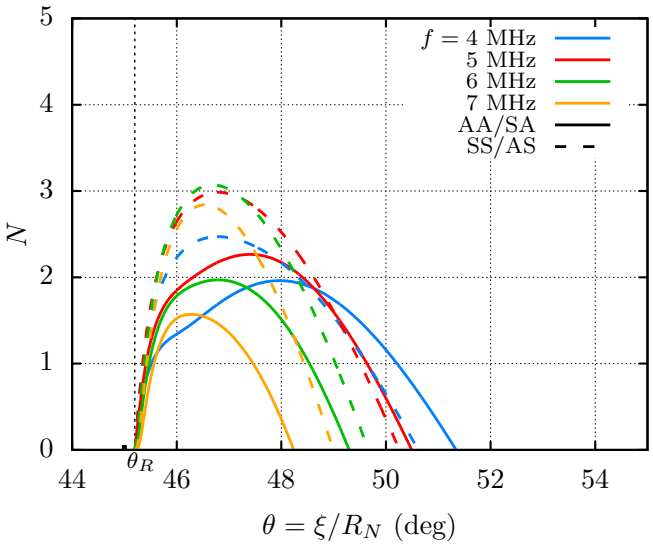

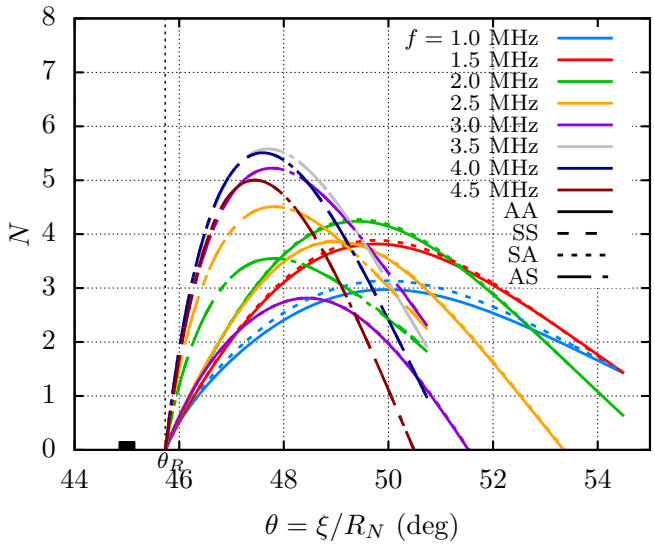

- Disturbance amplification occurs within few degrees from the roughness element
- Highest growth rates at reattachment location (θ_R) for most amplified modes
- Cubic, 20 μm: Modest $N_{max} \approx 3$ for SS/AS with $f = 6.0$ MHz
- Prismatic, 20 μm: Larger $N_{max} \approx 5.6$ for SS/AS with $f = 3.5$ MHz

Plane-Marching PSE Analysis of Roughness Wakes

- Roughness elements at $\theta = 45^\circ$ with $m = 420$ on $R_N = 15.24$ mm cone
- **Stable and robust integration of PSE only downstream of separation region**
- N-factor curves for symmetric (SS, AS) and antisymmetric (AA, SA) modes
  - $k = 20$ μm, Cubic
  - $k = 20$ μm, Prismatic

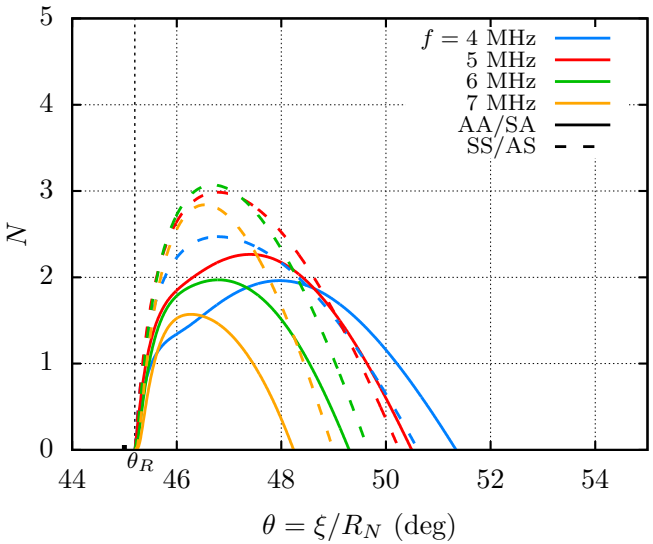

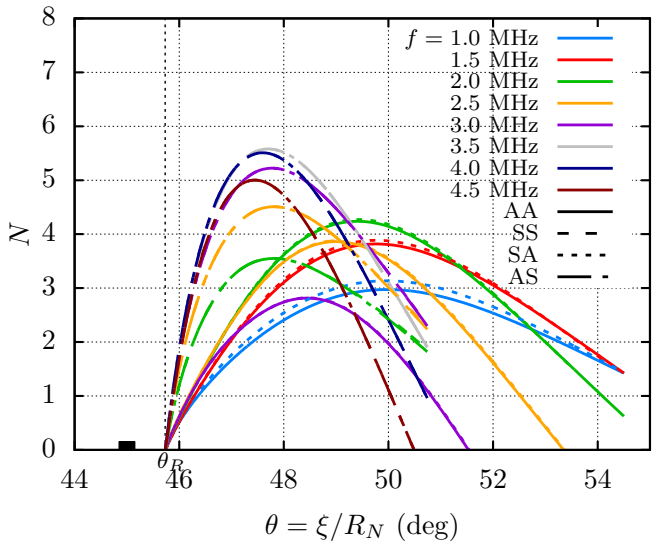

- Disturbance amplification occurs within few degrees from the roughness element
- **Highest growth rates at reattachment location (θ_R) for most amplified modes**
- Cubic, 20 μm: Modest $N_{max} \approx 3$ for SS/AS with $f = 6.0$ MHz
- Prismatic, 20 μm: Larger $N_{max} \approx 5.6$ for SS/AS with $f = 3.5$ MHz

Inflow-Resolvent HLNSE Analysis of Full Flowfield

- Prismatic roughness elements with $k = 20$ μm height
- Inflow set at $\theta_0 = 44.36°$ and optimization location at $\theta_1 = 47.4°$
- N-factor curves for symmetric (SS, AS) and antisymmetric (AA, SA) modes
  - Plane-marching PSE

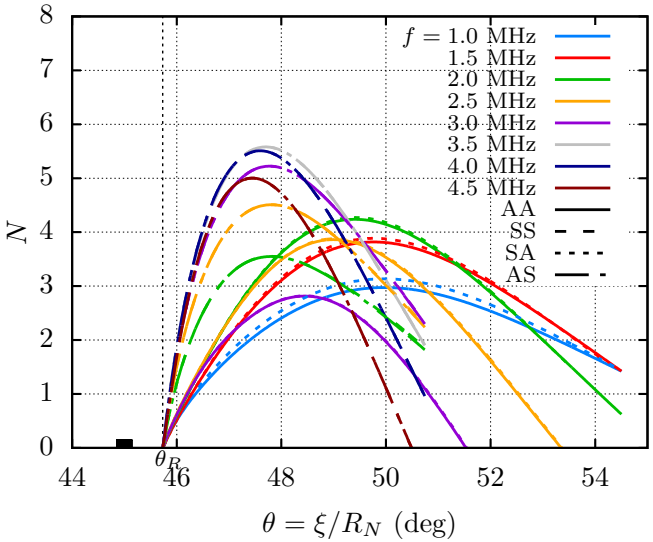

  - Inflow-resolvent HLNSE

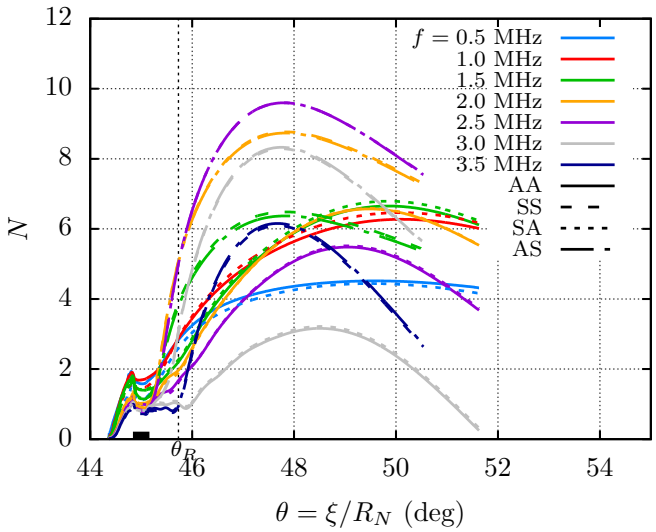

- Short region of amplification upstream of roughness elements due to transient growth
- Slight delay at roughness leading edge and grow again downstream of trailing edge
- Symmetric disturbances (SS, AS) experience earlier and stronger growth over separation
- $N_{max} \approx 9.6$ (71% higher than PSE) for AS/SS with $f = 2.5$ MHz (29% less than PSE)

Inflow-Resolvent HLNSE Analysis of Full Flowfield

- Prismatic roughness elements with $k = 20$ μm height
- Inflow set at $\theta_0 = 44.36^\circ$ and optimization location at $\theta_1 = 47.4^\circ$
- N-factor curves for symmetric (SS, AS) and antisymmetric (AA, SA) modes
  - Comparison of N-factor curves

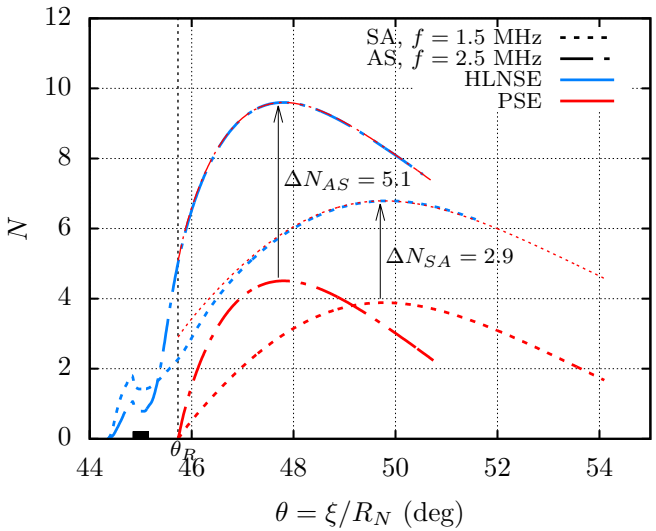

  - Comparison of spectra at $\theta = 48^\circ$

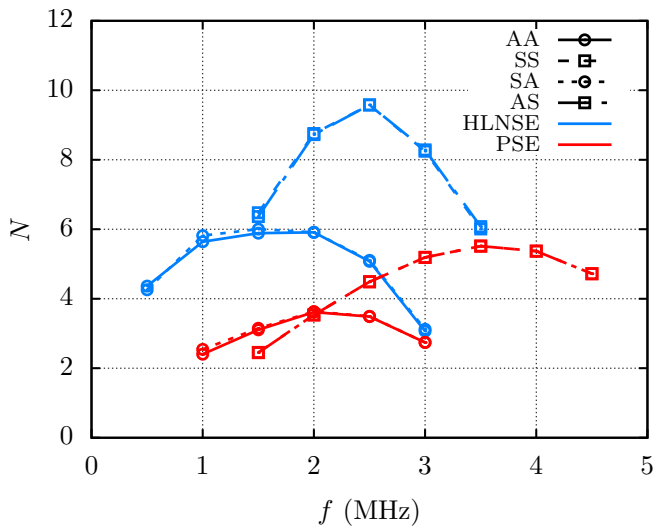

- Overlap by upward shift confirms HLNSE disturbances become modal streak instabilities
- HLNSE able to account for amplification over roughness element and separation region
- Rather significant shift in N-factor values and frequency bands for S and A modes
- Large difference between PSE and HLNSE predictions assumed to be due to strong favorable pressure gradient scenario (not observed for ZPG case[9])

[9] M. Choudhari et al. *Effect of 3D Roughness Patch on Instability Amplification in a Supersonic Boundary Layer*. AIAA Paper 2019-0877. 2019.

Inflow-Resolvent HLNSE Analysis of Full Flowfield

- Prismatic roughness elements with $k = 20$ μm height
- Inflow set at $\theta_0 = 44.36^\circ$ and optimization location at $\theta_1 = 47.4^\circ$
- Spatial structure of most amplified modes
  - SA, $f = 1.5$ MHz
  - AS, $f = 2.5$ MHz

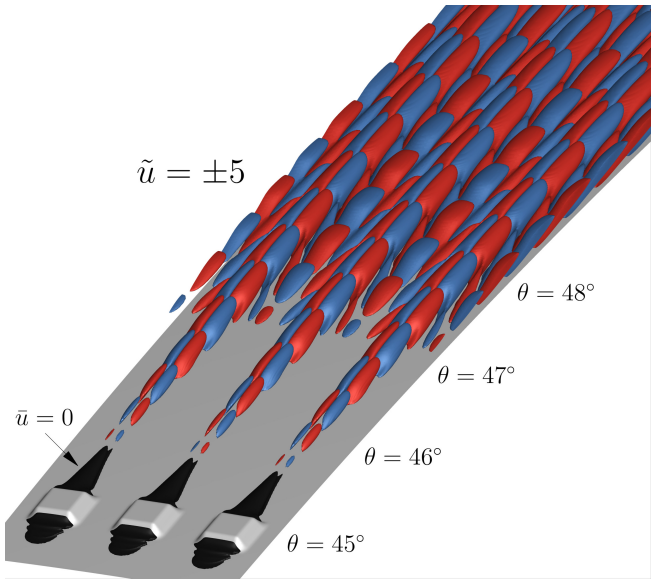

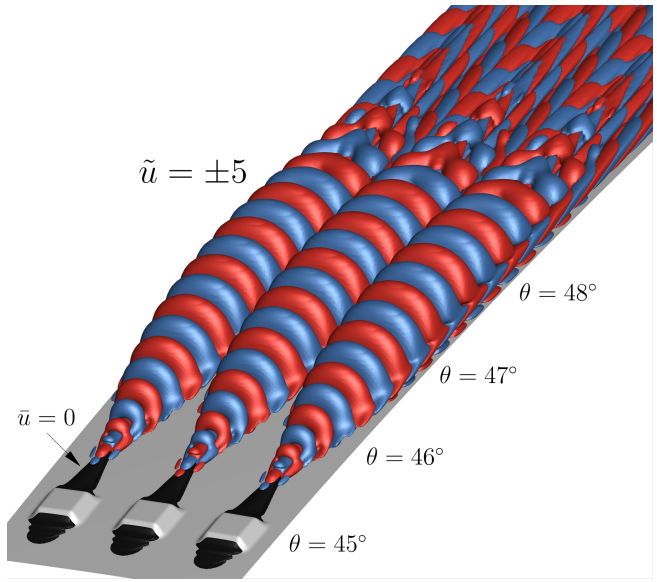

- Isosurfaces of $\tilde{u} = \pm 5$ normalized such $E_0 = 1$ and separation region ($\bar{u} = 0$)
- Shear layer over separated zone supports stronger growth of symmetric mode
- Amplification of symmetric mode terminates earlier
- Transition onset would occur within 3° downstream of roughness element

Outline

Summary and Concluding Remarks

- Effects of roughness height and planform shape are investigated by using cubic and prismatic elements with $k = 15$ μm ($k/\delta_h = 0.208$) and 20 μm ($k/\delta_h = 0.277$)
- Plane-marching PSE analysis of the roughness element wakes
  - insignificant $N_{max} = 0.16$ for experimental configuration (cubic 15 μm elements)
  - prismatic shape with 15 μm leads to $N_{max} = 1.9$
  - modest $N_{max} = 3$ and $N_{max} = 5.6$ for cubic and prismatic 20 μm elements
- Inflow-resolvent HLNSE analysis of entire flow field for 20 μm prismatic elements
  - extra amplification captured by the HLNSE in the vicinity of the roughness element including flow separation
  - predicts $N_{max} = 9.6$ that represents an increase of nearly 71% with respect to PSE
  - most amplified frequency predicted at $f = 1.5$ MHz (29% lower than PSE analysis)
- Future testing will be conducted at Purdue's Boeing/AFOSR Mach 6 Quiet Tunnel (BAM6QT) in both quiet, low-noise conditions and conventional noisy conditions for similar nosetip Reynolds numbers

Thank you for your attention

- Acknowledgments
  - This research was sponsored in part by the NASA Hypersonic Technology Project (HTP) under the Aeronautics Research Mission Directorate (ARMD) and by the U. S. Office of Naval Research (ONR) under award number N00014-20-1-2261 with P.O. Eric Marineau.
  - Resources supporting this work were provided by the DoD High Performance Computing Modernization Program, the NASA High-End Computing (HEC) Program through the NASA Advanced Supercomputing (NAS) Division at Ames Research Center and the NASA K-Midrange Cluster at Langley Research Center.